Semiconductor Physics, Quantum Electronics & Optoelectronics, 2017. V. 20, N 3. P. 284-296.
doi: https://doi.org/10.15407/spqeo20.03.284

PACS 78.20.-e, 78.66.-w

Ellipsometry and optical spectroscopy of low-dimensional family TMDs

V.G. Kravets[1], V.V. Prorok[2], L.V. Poperenko[2], I.A. Shaykevich[2]
[1]*School of Physics and Astronomy,*
University of Manchester, Manchester, M13 9PL, UK
[2]*Taras Shevchenko National University of Kyiv,*
Department of Physics
4, Prospect Glushkova, 03187 Kyiv, Ukraine

Abstract. Here, we report a comprehensive study of fundamental optical properties of two-dimensional materials. These properties have been ascertained using spectroscopic ellipsometry, optical spectroscopy of Raman scattering, and photoluminescence. We have focused on optical properties of the chemically exfoliated layered TMDs: MoS_2, $MoSe_2$, WS_2, and WSe_2. The complex refractive index and optical conductivity within the region 1 to 4.5 eV were extracted, which lead to identification of many unique interband transitions at high symmetry points in the electron band structure. The positions of the so-called A and B excitons in monolayers are found to shift upwards in energy as compared with those of the bulk form and have smaller separation because of the decreased interactions between the layers. For monolayer TMDs, the valence-band spin-orbit splitting at the K point was estimated from the energy difference between the A and B exciton peaks. Our findings of the spin-orbit coupling of ~0.16, ~0.26, ~0.37, and ~0.55 eV in monolayers MoS_2, $MoSe_2$, WS_2, and WSe_2, respectively. All these findings not only extend our understanding the novel electronic structures of mono- and few-layers TMDs but also provide foundation for future technological applications of optoelectronic and spintronic device components.

Keywords: ellipsometry, optical spectroscopy, low-dimensional structures, transition metal dichalcogenides.

Manuscript received 11.07.17; revised version received 03.08.17; accepted for publication 06.09.17; published online 09.10.17.

1. Introduction

Graphene, a single layer of carbon atoms, presents a range of unusual properties that sparked interest in two-dimensional (2D) materials. Nowadays, it is probably fair to say that research on graphene has already started to shift from studying graphene itself to the use of the 2D materials in applications [1, 2]. Indeed, 2D monolayers have received a great deal of interest over the past 10 years, as they show great promise for revolutionizing many areas of physics. The term monolayer refers to solid materials with minimal thickness: occasionally, as with graphene, a monolayer is only one-atom thick, but in crystals they can comprise three or more atomic layers. Low-dimensional materials frequently exhibit unexpected properties that make them as interesting for research, with the so-called transition metal dichalcogenides (TMDs) providing particularly

promising [3-6]. Usually, TMDs consist of a large family of materials with the general form TX2, where T is a transition-metal from the 4th to 6th group of the Periodic Table and X is a chalcogen – sulphur, selenium, or tellurium. In general, TMDs formed by metals from the 4th and 6th groups are usually semiconductors. While the bulk of the material has an indirect band gap, single and few layers TMDs are a direct-gap semiconductor [3-6]. Semiconductors with a direct gap are of special interest for use in optics and optoelectronics. Layered semiconductor TMDs have proven to be important candidates for use as an absorber layer in low cost thin film solar cells [7-9]. This is due to their relatively small band gap (~1–2 eV) and the large absorption coefficient (about 10 % in visible rage). Moreover, TMDs are also capable to generating light by supplied energy. Monolayers have two surfaces and no bulk between them, which presents the extreme case of surface science. To study the specificity of surface electronic states, the spectroscopic ellipsometry (SE) is a powerful non-destructive technique that enables to collect information about optical properties of low-dimensional materials. Optical constants extracted from ellipsometric measurements represent a versatile approach for probing the surface electronic structure of materials [10, 11]. SE allows obtaining simultaneously both the real (n) and imaginary (k) parts of the complex refractive index in contrast to other optical techniques such as transmission and reflection spectroscopy. For optoelectronic device applications of TMDs monolayers to be fully understand, it is also necessary to know the complex refractive index and then to determine optical conductivity. Recently, we have employed the SE to investigate the optical constants of graphene [12, 13], however, up to date, SE characterisation of 2D layered TMDs has rarely been reported [14-16]. Moreover, additional UV-visible-near-infrared absorption measurements can promote deepening the understanding of the optical response of 2D systems for successful nanooptical device engineering.

Here we report the optical characteristics of layered materials that are exfoliated in liquids using a combination controlled ultrasound sonication and centrifugation. In this process, mono- and few-layers TMDs nanosheets could be obtained. It was found that optical and electronic properties of these low-dimensional structures are determined by the strong confinement of charge carriers in a 2D plane. As a consequence, the 2D confinement of electrons upon chemical exfoliation leads to intriguing optical and electronical properties. The strong electrostatic interactions give rise to electron-hole pairs in these materials, called as exciton. The ellipsometric method allows studying such excitons in details: to determine their energy of excitation and intensity. Knowing and deep understanding the optical properties of mono- and few-layers TMDs as well as integrating them with light interaction are an important step in creating a materials platform for solar energy accumulation.

In our study, we have focused on optical properties of such layered transition metal dichalcogenides as MoS_2, $MoSe_2$, WS_2, and WSe_2. It was carried out independent ellipsometric and transmission measurements to determine the optical constants as well as high frequency conductivity of mono- and few-layers TMDs nanosheets. We discuss the energy location and nature of the main optical peaks appearing in the spectra of chemically exfoliated monolayers and thick (bulk) specimens. Our experimental results reveal qualitative agreement among all four monolayer complex refractive indexes ($n^* = n + ik$) and their corresponding to the bulk values. We also manifest the differences in optical spectra occurred due to blueshifts of the A and B excitons, resulting in enhancements of the exciton binding energy, as well as increases of monolayer bandgaps. It is important to note that investigated mono- and few-layers TMDs exhibit an indirect-to-direct bandgap transition, due to this they possess strong photoluminescence emission at room temperature. In this work, the valence-band spin-orbit splitting at the K point of the Brillouin zone was extracted being based on the energy difference between the A and B exciton peaks.

2. Samples preparation and experimental methods

Exfoliation of monolayers and few layers of TMDs from its bulk remains a challenge due to their natural tendency to form stacked structures. There are a number of techniques presented in the literature for the synthesis of monolayers of TMDs, *i.e*. mechanical exfoliation, wet chemical approaches, physical vapor deposition, chemical vapor deposition (CVD), sulfurization of metal films and liquid exfoliation [17]. Among these methods, the liquid exfoliation route seems to be effective, particularly for sensing and solar cells applications, where a large quantity of nanosheets with inherent defects is required. Note that the surface of TMDs that are exfoliated in high yield solvents, namely: N-Methyl-2-pyrrolidone (NMP), polymer solutions, or surfactant solutions, are not pristine. These solvents and co-solutions are hard to remove as they occupy the surfaces of the exfoliated nanosheets [18].

In this work, we have exfoliated TMDs via sonication in a mixture of ethanol and 3% vol. anisole (analogy of poly(methyl methacrylate) solving). These solvents have low boiling points, hence the exfoliated nanosheets are pristine and no extra process steps are required to remove these solvents. The sonication time was approximately 20 hours. During long time sonication process, a transverse component of ultrasonic waves is able to overcome the van der Walls weak interlayer interactions. In this process, mono- and few-layers TMDs nanosheets along with a large fraction of small TMDs nanocrystals could be obtained. Then, the exfoliated TMDs solutions are divided into several 10 ml by centrifuge tubes and centrifuged for 10 min at 10,000 rpm to remove any remaining nanocrystals. The

high-speed centrifugation process leads to separation of variable sized nanocrystals. To measure the nanosheets thickness, we deposited a few drops of TMDs dispersion onto Si/SiO_2 (1-2 nm oxide thickness) before drying in air followed by characterising with scanning electron microscopy (SEM) and profilometry. The resulting TMD nanosheets were mostly single and few-layered (sheet thickness ~1.0 to 4 nm) with lateral dimensions of 200…1000 nm. For optical characterization of the investigated TMDs monolayers, small volumes of diluted TMDs suspensions were drop-coated onto smooth silica substrates and then dried before measurements. As a bulk samples, we used specimens obtained directly from dried drop of starting powder solutions (without sonication and centrifugation). In order to improve semiconducting properties, the 2D monolayer films were annealed at $T = 250$ °C for 3 hours in argon atmosphere. Initial materials MoS_2, $MoSe_2$, and WS_2, WSe_2 (99.8%, Metal basis) micrometer powders were purchased from Alfa Aesar.

The structural characterization and the sheet size distribution were measured by SEM. Due to long time ultrasonication, all the TMDs nanosheets are found to be smaller than 1.0 μm in nominal size. Spectral ellipsometric measurements were performed with a light photon energy from 1.0 to 4.5 eV applying Beattie technique [19-21]. The azimuth of the restored polarization Ψ and the phase shift Δ between *p*- and *s*-components of a polarization vector **E** were measured at different values of light incidence angle θ from 55° to 75° with the step of 5 deg. The spot size on the sample was approximately 1.0 mm in diameter, which allowed averaging characteristics of the sample from a large area. The ellipsometric parameters Ψ and Δ are defined as $\tan(\Psi)\exp(i\Delta) = r_p / r_s$, where r_p and r_s are the reflection coefficients for the light of *p*- and *s*-polarizations [17, 18]. The three-phase ellipsometric model consisting of the substrate (silica), thin film (MoS_2, $MoSe_2$, and WS_2, WSe_2), and ambient (air) was employed to extract the complex refractive index of corresponding TMDs film. We fitted the experimental curves of ellipsometric angles Ψ and Δ to theoretical ones using the abovementioned model and calculated the Fresnel reflection coefficient [10, 12, 13, 20]. As a result, the optical constants and high frequency conductivity were calculated under assumption of their isotropy and homogeneity. The mean squared error (MSE, a measure of the goodness of fit of the model to the data) was low (below 7-8). It has to be noted that the values of the TMDs film thickness were used as parameters on the initial stage of fitting and correspond to the data of the thickness measured by a Talystep profilometer. The thickness distribution for TMDs is obtained by scanning a samples area of 1×1 mm^2. The assembly of mono- and few-layers TMDs films, for which we presented optical data below, had the thickness about 50…70 nm. More precise values of the thickness and the complex refractive indexes ($n^* = n + ik$) of layered TMDs nanosheets were obtained after fitting the experimental angle dependent Ψ and Δ functions [10-12, 20]. Optical constants of bulk TMDs layer (with the thickness about 1 mm) were calculated directly by applying Airy's formula with the ellipsometric parameters Ψ and Δ for different angles of incidence [13, 20]. The optical conductivity for TMDs can be found as follows: $\sigma(\omega) = nk\omega/2\pi = \varepsilon_2(\omega)\omega/4\pi$ (where ω is the light frequency, and $\varepsilon_2(\omega)$ – imaginary part of the dielectric function). Note that in general the optical conductivity, $\sigma(\omega)$, and the imaginary part of the dielectric function, $\varepsilon_2(\omega)$, are tensors. Here, we assume for simplicity that the medium is isotropic, so that the conductivity $\sigma(\omega)$ and the dielectric complex function $\varepsilon(\omega)$ are scalars. We have defined the complex dielectric function and the real part of optical conductivity as given in [21-24].

Additionally, UV-visible-near-infrared grating spectrometer with a xenon lamp source was used for measuring the absorption spectra of monolayers. In cases where scattering is negligible, light attenuation is dominated by absorption, and the transmitted intensity, $I(t)$, is related to the sample absorption coefficient, $\alpha_{abs} = 4\pi k/\lambda$ via the Beer–Lambert law: $I(t) = I_s \exp(-\alpha_{abs} t)$. Here, I_s is the incident light intensity (normalized to transmission of pure silica substrate), and t is the thickness of assembly of monolayers. Note that the thickness of each sample was measured by using angle-variable SE. Raman and photoluminescence measurements were performed using a Renishaw Raman system with 514.5 nm argon laser. Typically, the samples were measured using (50) 100× lens, and the laser beam was focused into ~1 μm diameter spot.

3. Results and discussion

Optical properties of MoS_2 films. MoS_2 mono- and few-layers were identified by SEM as well as photoluminescence (PL) and Raman spectroscopy. The SEM image in Fig. 1a reveals a layer-by-layer assembly of corresponding monolayes. The Raman analysis of the samples allows having an insight on the crystal structure and dimension of our samples. Raman spectrum of thick (bulk) MoS_2 consists of two well-known Raman bands at ~383 and ~408 cm^{-1} that correspond to E^1_{2g} and A_{1g} vibrational modes (Fig. 1b) [25-27]. It is evident that the E^1_{2g} and A_{1g} peaks shift closer to one another with decreasing the film thickness, which is an excellent indicator for the number of layers in MoS_2 [26, 27] . In the case of thick film, the E^1_{2g} and A_{1g} peaks are separated by ~25 cm^{-1}, whereas for mono- and few-layers, the same peaks manifest themselves at ~386 and ~405 cm^{-1} with separation of ~20 cm^{-1}. The increase of the frequency difference in bulk MoS_2 is caused by the influence of neighbouring layers on the effective restoring force on atoms as well as the increase of dielectric screening of long-range Coulomb interactions [25-27].

Semiconductor Physics, Quantum Electronics & Optoelectronics, 2017. V. 20, N 3. P. 284-296.
doi: https://doi.org/10.15407/spqeo20.03.284

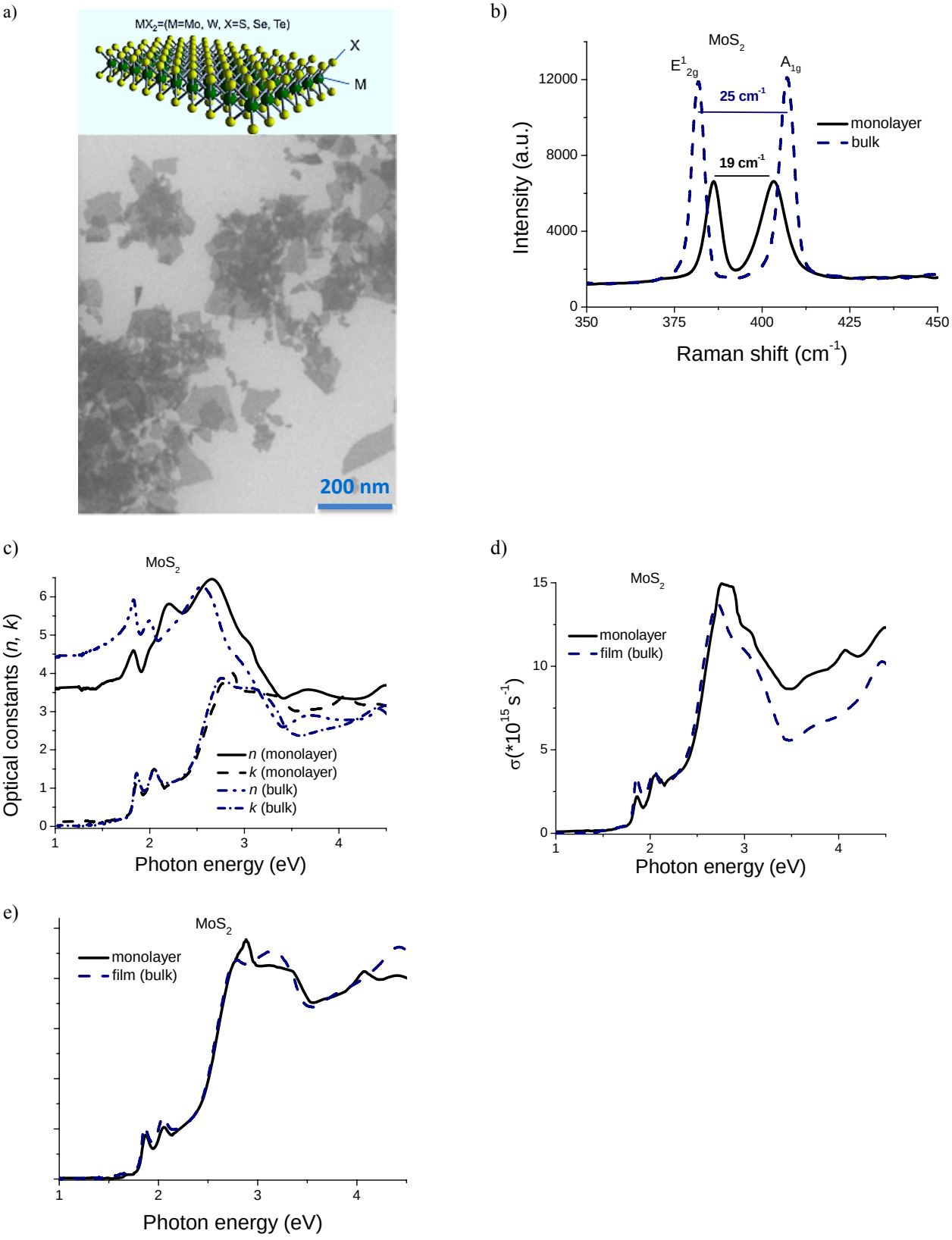

Fig. 1. Optical properties of mono- and few-layers MoS_2 nanosheets. (a) SEM image of mono- and few-layers MoS_2 nanosheets (Inset: schematic structure of the TMD monolayers). (b) Raman spectra of low-dimensional MoS_2 nanosheets and bulk films. (c) Extracted optical constants from ellipsometric measurements for mono- and few-layers MoS_2 and bulk films. (d) Optical conductivity of MoS_2 nanosheets and bulk films. (e) Changes of absorption spectra α_{abs}, when one moves from mono- and few-layer MoS_2 to the bulk state.

Figs 1c and 1d show the spectra of the complex refractive index and optical conductivity of the MoS_2 mono- and few-layers and bulk samples. Two dominant peaks are observed at the energies ~1.88 and ~2.04 eV in the *k* and σ(ω) plots in the red region. We can see that, for smaller wavelengths, the real and imaginary parts of the refractive index of low-dimension MoS_2 are both higher than their bulk counterparts. Two spectral regions with dominant absorption variations are observed in the photon energy range of 1.5…3.8 eV, which are related to A, B excitonic peaks in the range of 1.8…2.5 eV, and C, D excitonic peaks in the range of 2.7…3.3 eV, respectively [28]. The plots of absorption coefficient, α_{abs} (Fig. 1e) shows good agreement with these two peaks observed at the energies ~2.0 and ~3.0 eV in the *k* (σ(ω)) spectra. We found that mono- and few-layers MoS_2 displays an extraordinary large value of the refractive index about ~6 at ~3 eV. In addition, for monolayer MoS_2, two peaks of the imaginary part of the refractive index spectrum exhibit a slightly blue shift compared to their bulk counterparts. The observed blue shifts of exciton absorption of monolayer MoS_2 as compared to their bulk counterparts may be caused by the difference of A and B excitons energy in bulk and mono- and few-layers MoS_2. There also exists a peak near ~3 eV for the imaginary part spectrum of monolayer MoS_2, which may be related to the Van Hove singularities or C and D excitons [29]. It is interesting to note that our measurements of the optical properties of MoS_2 monolayer are consistent with the main feature of the electronic band structure calculated in [28]. The appearance of two distinct low-energy peaks in the absorption spectrum, commonly referred to as the A and B excitons, are the result of electron transitions between the valence splitted band and the conduction band [28]. It can be seen that there is a general similarity of exciton peaks in *k*, α_{abs} and σ(ω) spectra (Figs. 1c-1e). They indicate that the energy difference between exciton B and A peaks is equal 2.04–1.88 = 0.16 eV, which corresponds to the spin-orbit splitting at the K point of the Brillouin zone [28]. This value is in good agreement with previous calculations [28] of ~0.15 eV. Thus, we see the appearance of two distinct absorption peaks in monolayer MoS_2 at 1.88 and 2.04 eV, which correspond to the strongly bound A and B excitons, respectively.

Optical properties of WS_2 films. SEM image of chemically exfoliated mono- and few-layers WS_2 flakes with a small thickness is presented in Fig. 2a. The most powerful method to confirm monolayer's origin of WS_2 is Raman spectroscopy (see Fig. 2b). This plot displays thickness-dependent evolutions of the E^1_{2g} and A_{1g} Raman active modes. For WS_2 monolayer, the E^1_{2g} mode exhibits slightly red shifts, while the A_{1g} mode – blue shifts. Our measurements confirm the results of [25, 27] and show that the difference between frequencies of A_{1g} mode and E^1_{2g} mode in the case of WS_2 can also allow the identification of the thickness of WS_2 flakes similar to MoS_2. The distinction between WS_2 and MoS_2 is that the frequency difference of Raman modes for WS_2 is ~63 cm^{-1}, *i.e.*, about three times larger than that for MoS_2, which is related to the larger mass of W than Mo. It leads to a larger frequency gap between Raman active modes.

Optical transitions between the split valence band and the conduction band give rise to distinct low-energy peaks in the spectra of optical constants *n* and *k* (Fig. 2c) commonly referred to as A excitons. One can clear see the appearance of only one pronounced absorption peak at ~2.05 eV, which correspond to the strongly bound A excitons [28]. Figs 2d, 2c display the spectral dependences of σ(ω) and α_{abs} for mono- and few-layers WS_2 with its associated bulk values. Note that single and few-layers optical responses qualitatively resemble their bulk counterparts for MoS_2 and WS_2 (Figs. 1c-1e and 2c-2e). However, in the case of WS_2 monolayer, α_{abs}, σ(ω) and *k* related with A exciton are better defined. This behaviour is rationalized by exciton binding energy enhancement caused by the confinement effect in monolayer TMDs (1.1 eV in the case of monolayer as compared with 0.1 eV in bulk) [28], which increases absorption efficiency. From our measurements, we can conclude that there are two types of electron transitions: i) between the valence band (top) and conduction-band minimum at K, which leads to A-type excitons (~2.05 eV) in the absorption spectrum, and ii) from the valence band (bottom) and conduction-band minimum at K, which leads to B-type excitons (~2.43 eV) less pronounced in the absorption spectrum.

Optical properties of $MoSe_2$ films. At the first stage, the monolayer's nature of $MoSe_2$ was identified by SEM imaging (Fig. 3a), as well as Raman spectroscopy (Fig. 3b). For a mono- and few-layers $MoSe_2$, only one Raman active out-of-plane mode (A_{1g}, see Fig. 3b) appears, since the unit cell contains only one $MoSe_2$ molecule, and no translation symmetry along the *c* axis exists. For a bilayer with two $MoSe_2$ molecules per unit cell the situation is similar to bulk material with only one Raman active out-of-plane mode [30]. More interestingly, the intensity ratio between the A_{1g} and E^1_{2g} Raman active modes (I_{A1g}/I_{E2g}) changes from ~5…10 for bulk up to ~20…30 for the monolayer $MoSe_2$ while the ratio remains nearly constant (~1.1) in the MoS_2 case (Fig. 1b). However, the mode shifts towards higher wavenumbers as compared to the monolayer due to the interlayer interaction. In the case of bulk $MoSe_2$, the A_{1g} mode shifts about 150 cm^{-1} towards lower wavenumbers as compared to MoS_2 (Figs. 1b and 3b), which is also confirmed by calculations [30]. As concerning MoS_2, we find the characteristic softening of the mode E^1_{2g} with decreasing the thickness of material. It amounts to ~3 cm^{-1} from bulk to monolayer $MoSe_2$. Our measurements are in good agreement with recent studies where the main Raman peak at 243 cm^{-1} on a mechanically exfoliated $MoSe_2$ monolayer was reported [31].

Semiconductor Physics, Quantum Electronics & Optoelectronics, 2017. V. 20, N 3. P. 284-296.
doi: https://doi.org/10.15407/spqeo20.03.284

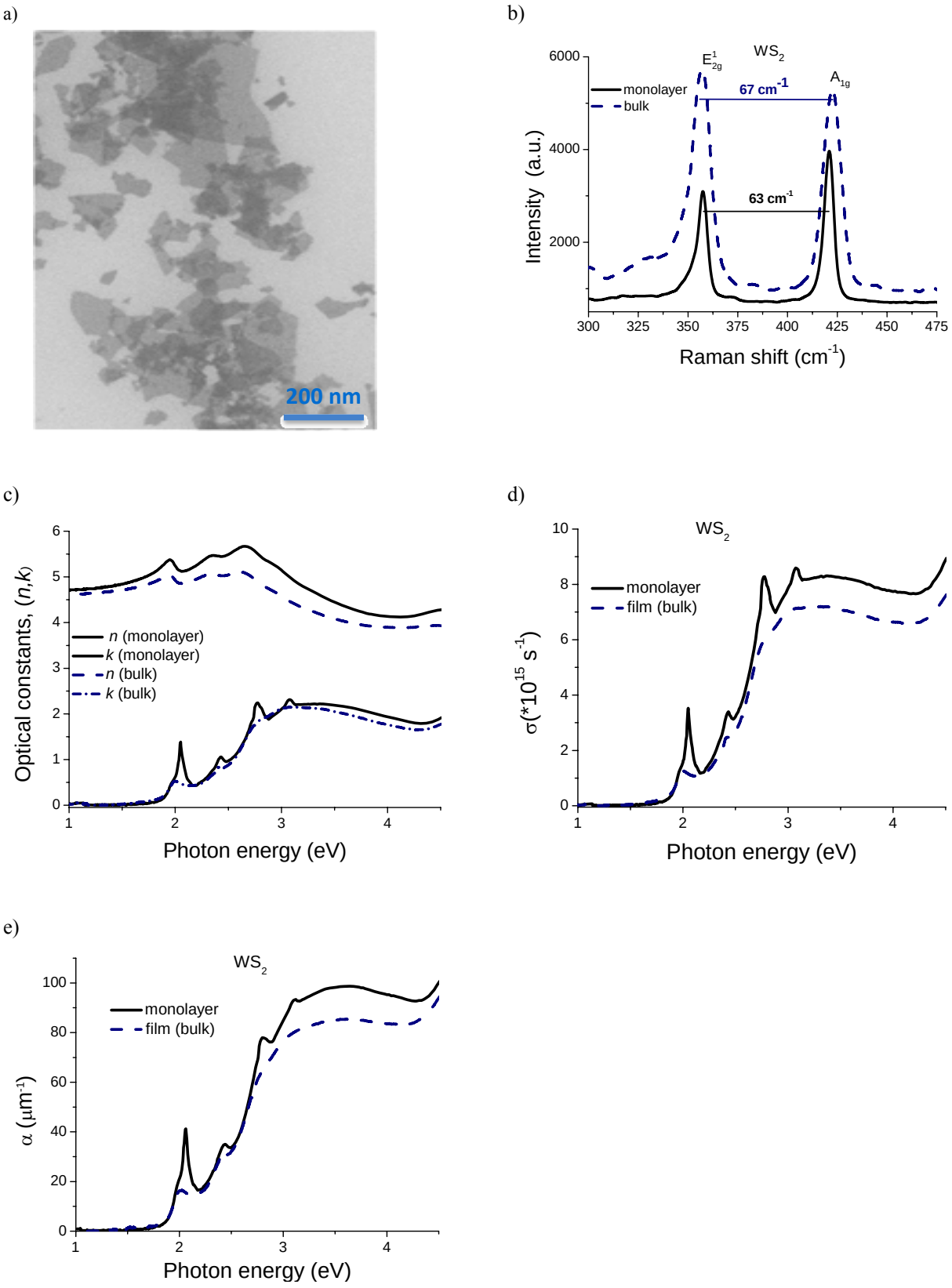

Fig. 2. Optical properties of mono- and few-layers WS_2 nanosheets. (a) SEM image of mono- and few-layers WS_2 nanosheets. (b) Raman spectra of low-dimensional WS_2 nanosheets and bulk films. (c) Extracted optical constants from ellipsometric measurements for mono- and few-layers WS_2 and bulk films. (d) Optical conductivity of WS_2 nanosheets and bulk films. (e) Changes of absorption spectra α_{abs}, when moving from mono- and few-layers WS_2 to the bulk state.

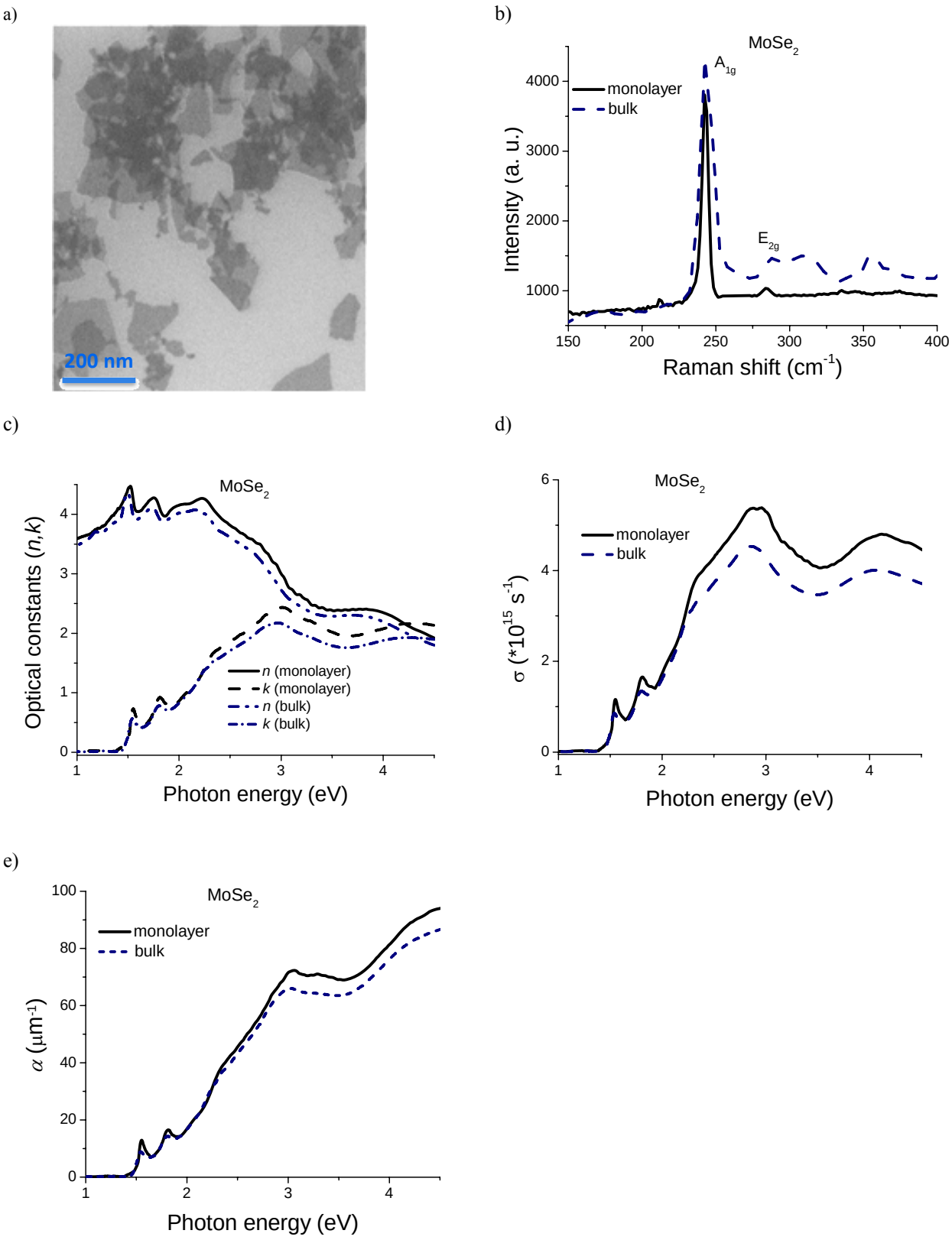

Fig. 3. Optical properties of mono- and few-layers $MoSe_2$ nanosheets. (a) SEM image of mono- and few-layers $MoSe_2$ nanosheets. (b) Raman spectra of low-dimensional $MoSe_2$ nanosheets and bulk films. (c) Extracted optical constants from ellipsometric measurements for mono- and few-layers $MoSe_2$ and bulk films. (d) Optical conductivity of $MoSe_2$ nanosheets and bulk films. (e) Changes of absorption spectra α_{abs}, when moving from mono- and few-layers $MoSe_2$ to the bulk state.

The refractive index, *n*, extinction coefficient, *k*, optical conductivity σ(ω), and absorption coefficient α_{abs} spectra of mono- and few-layers and bulk $MoSe_2$ are plotted in Figs. 3c-3e, respectively. For low-dimensional $MoSe_2$, the absorption part of the spectra for *k*, σ(ω) and α_{abs} are dominated by two peaks around 1.55 and 1.81 eV, which come from the A and B exciton transitions [28]. A and B excitons are formed at the K point of the Brillouin zone, where strong spin-orbit coupling induces a splitting in the opposite spin valence bands by about (1.81–1.55 = 0.26 eV) from our measurements. The obtained value of spin-orbit splitting in the mono- and few-layers $MoSe_2$ is in excellent agreement with previous calculations [28] of ~0.25 eV and is larger than that for MoS_2 (~0.16 eV). Note that for bulk $MoSe_2$ the corresponding two exciton transition peaks are weaker and exhibit small red shifts (Figs. 3c-3e). The A, B exciton peaks observed in this energy range occur before the onset of strong interband transitions near ~3 eV. Moreover, for layered $MoSe_2$ several peaks of the real part of the refractive index, *n*, locate in high-energy region as compared to the spectra of bulk (Fig. 3c). Note that the energy of A and B excitons for single and few-layers $MoSe_2$ is well matched to the solar spectrum, which can open up a new direction for 2D-materials applications as extremely thin film for new generation of solar cells.

Optical properties of WSe_2 films. The SEM image shown in Fig. 4a demonstrates the uniformity of WSe_2 sheet coverage on Si substrate. For bulk WSe_2, we found distinct Raman signals at ~250 and ~260 cm^{-1} (shoulder) and a small feature at 309 cm^{-1} (Fig. 4b). These three lines are also in agreement with the recent calculation [30] predicting both the E^1_{2g} and A_{1g} mode to be close to ~250 cm^{-1}. For mono- and few-layers WSe_2, we only detect a single maximum with a broad halfwidth at ~250 cm^{-1}.

The measured complex refractive index (Fig. 4c) and absorption coefficient (Figs. 4d, 4e) of mono- and few-layers and thick WSe_2 films indicate that the optical constants for layered nanostructure vary significantly with wavelength. Due to the high refractive indexes $n \approx 5…6$ in the visible frequency range the WS_2 and WSe_2 monolayers (Figs. 2c and 4c) can have many potential applications, such as good antireflection coatings for photonics and optoelectronics, and optical encapsulation for the enhancement of photovoltaic cell response [32]. The absorption spectra can be divided into a region at low energies, which are dominated by excitonic transitions on a relatively low absorption background and a region of strong absorption at higher energies. The extinction coefficient, *k*, absorption α_{abs}, and conductivity, σ(ω), for WSe_2 (Figs. 4c-4e) show peaks at ~1.65 eV and ~2.20 eV, respectively, which corresponds to the A, B band transitions due to splitting of the ground and excited states in the WSe_2 electronic structure [28].

Common features and differences in optics of low-dimensional TMDs. The comparison of the complex refractive indexes ($n^* = n + ik$) for MoS_2, WS_2, $MoSe_2$, and WSe_2 reveals qualitative agreement between all four monolayer dielectric functions and their corresponding bulk values. For monolayers, the most prominent features in the spectra are a series of sharp peaks in the lower energy range ($E < 2.5$ eV), and a series of broad and low oscillations at higher photon energies ($2.5 < E < 4.5$ eV). The derived optical constants *n* and *k* initially show strong dispersion and absorption associated with the spin-orbit split exciton pair A and B. The structure is sharper, better resolved and more intense for the sulphide monolayers than for the selenide ones, as observed in ellipsometry and transmission measurements. The excitonic absorption peaks A and B, which arise from direct gap transitions at the K point, are found in agreement with the previous studies of bulk [33] and monolayer samples [34, 35]. The energy difference between the A and B peaks, which is indication of the strength of spin-orbit interaction, is in reasonable agreement with the calculations [28, 35]. For monolayer TMDs, the valence-band spin-orbit splitting at the K point can be estimated from the energy difference between the A and B exciton peaks. Our findings of the spin-orbit coupling of ~0.16, ~0.26, ~0.37, and ~0.55 eV in low-dimensional MoS_2, $MoSe_2$, WS_2, and WSe_2 are consistent with the previous theoretical predictions [28] and differential reflectance spectroscopies for mechanically exfoliated monolayer WS_2 and WSe_2 [36]. Note that, due to the theory, the spin-orbit splitting energy increases as the fourth power of the average atomic number of the constituent elements, leading to the giant spin-orbit splitting (~0.55 eV) in monolayer WSe_2 [28]. The observed blueshifts of the exciton energies with decreasing the TMDs nanosheet size and their energy behaviour can be ascertained using the quantum-confinement approach [26, 37]. Lower energy excitons (A and B) are originated from electron transitions between the valence and conductive bands in the vicinity of the K point (Brillouin zone). The electron densities of states in the K point are composed primarily from the transition metal *d* orbitals [15]. Consequently, the A and B excitons are spatially localized in the plane of the metal atoms [15, 38]. Due to this fact, they are stable in monolayer semiconductors, and their energy do not change significantly. The high energy ($E > 2.5$ eV) features are, however, associated with transitions away from the K point and involves significant contribution from the chalcogen orbitals (2*s* and 2*p*) [27, 28], which causes larger energy shifts. An additional difference is that the magnitude of the real part of refractive index, *n*, is generally larger than that of the corresponding bulk. It is most pronounced in the case of WS_2 (Fig. 2c), $MoSe_2$ (Fig. 3c) and WSe_2 (Fig. 4c) likely arises from dielectric environment differences between bulk and single layer specimens. The extinction coefficient, *k*, in the region 3 to 4.5 eV is about ~2.5…3.5, which is comparable with

Semiconductor Physics, Quantum Electronics & Optoelectronics, 2017. V. 20, N 3. P. 284-296.
doi: https://doi.org/10.15407/spqeo20.03.284

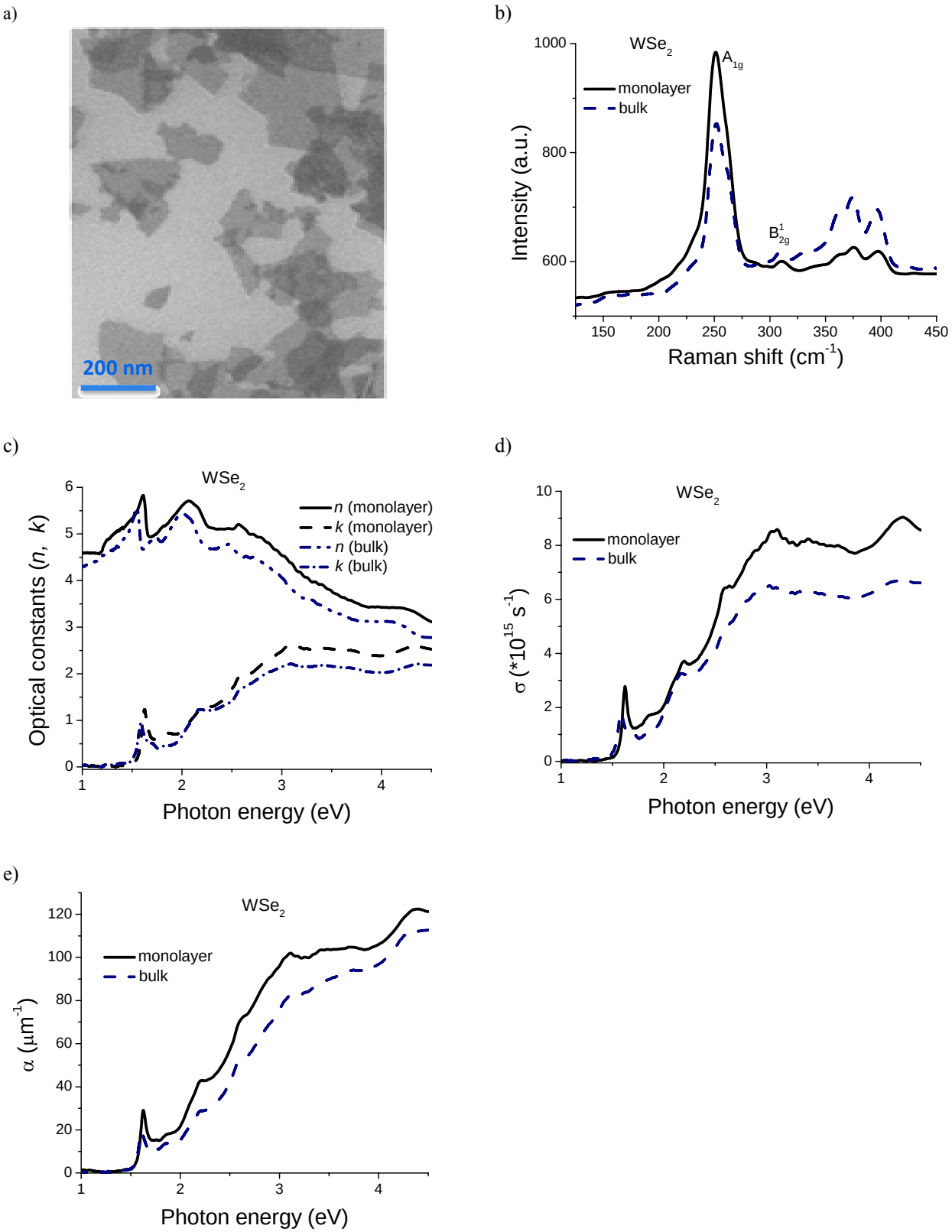

Fig. 4. Optical properties of mono- and few-layers WSe_2 nanosheets. (a) SEM image of mono- and few-layers WSe_2 nanosheets. (b) Raman spectra of low-dimensional WSe_2 nanosheets and bulk films. (c) Extracted optical constants from ellipsometric measurements for mono- and few-layers WSe_2 and bulk films. (d) Optical conductivity of WSe_2 nanosheets and bulk films. (e) Changes of absorption spectra α_{abs}, when one moves from mono- and few-layers WSe_2 to the bulk state.

that (~3.2) of Yim *et al*. [14] for ultrathin CVD MoS_2 and with the data of Li *et al.* [15] for TMDs, but much lower than that (~5.1) of Shen *et al*. [39]. The higher coefficient, *k*, could be a result of sample structural quality or the way it was extracted from their four-phase ellipsometric model [39].

It is well known that the optical conductivity spectra σ(ω) reflect the main details of the density of electron states within energies close to critical points (CPs) [40]. The CP dimension is classified being based on the electron energy dispersion at Van Hove singularities, which can be expanded as a function of the momentum vector **k** about CP as $E(k) = E(0) + \alpha_1 k^2_1 + \alpha_2 k^2_2 + \alpha_3 k^2_3 + \ldots$, where the dimension is assigned by the number of nonzero coefficients α, for 2D represent two, nonzero α [40]). The optical conductivity σ(ω) derived from the imaginary part of the dielectric function and absorption coefficient α_{abs} extracted from transmission measurements for mono- and few-layers and bulk TMDs (Figs. 1-4 (c, d)) demonstrate higher values for the monolayer. The optical conductivity reflects main features of the joint density-of-states function $J(E) \propto E\varepsilon_2(\omega) = \sigma(\omega)$ and are, perhaps, the most relevant to studies of the band structure of monolayers. A series of fine resolved peaks in σ(ω) spectra at a higher energies than these of A and B excitons are clearly observed for TMDs, which can be attributed to optical transitions along the parallel bands between the M and Γ points in the reduced Brillouin zone. In the ultraviolet region, singularities in σ(ω) are also observed and can be associated with a combination of several critical points as seen for common semiconductors [40]. The structure within the range 2.5…4.5 eV is much stronger in terms of absorption in the sulphide than that in selenide. The shapes and positions of the gross features in the *J*(*E*) once again show the similarity between MoS_2 (WS_2) and $MoSe_2$ (WSe_2). This may be a direct result of similarity between the band structures for these materials, which supports the theoretical rigid-band model by Wilson and Yoffe (Ref. [33]). The striking difference between the Mo and W compounds can be qualitively understood for the following reasons: (i) the effect of chalcogen ligand field on metal "*d*" states increases with increasing the metal atomic number due to changes in the electronegativity and orbital radii; as a result, wider overlap of the "*d*" band with the "*s*-*p*" conduction band in these W compounds than in the Mo compounds has been produced; (ii) overlap between the outer orbitals of nearest-neighbour metal atoms is greater for the larger W atoms. Due to this, the widths of metal "*d*" and "*s*-*p*" conduction bands increase for W-base monolayers [33].

The extracted dielectric function, ε(ω), and optical conductivity, σ(ω), of chemically exfoliated mono- and few-layers TMDs can be modelled by fitting with multi-Lorentzian functions:

$$\varepsilon(\omega) = 1 + \sum_{k=1}^{N} \frac{f_k}{E_k^2 - E^2 - iE\gamma_k} \qquad (1)$$

where f_k, E_k, and γ_k are the oscillator strength, the spectral resonance energy E_k, and the spectral width γ_k of the *k*-th oscillator, respectively. The real part of the optical conductivity σ(ω) is related to the dielectric permittivity ε(ω) via the following relation: $\sigma(\omega) = \mathrm{Re}[i(1-\varepsilon(\omega))\omega]$ [24]. The values of the model parameters for the four investigated TMD monolayers were determined by fitting Eq. (1) to the experimental data presented in Figs. 1d-4d. A good agreement between the extracted experimental dependences of σ(ω) and the analytical formula (1) were obtained for the f_k, E_k, and γ_k parameters presented in Table. Note that the numerical fitting is less accurate for $E > 3.5$ eV due to possible contribution of the film roughness and additional impurities into the experimental data. The energy dependence of the real part of the optical conductivity for four TMD chemically exfoliated mono- and few-layers materials is depicted in Fig. 5a.

Table. Model parameters for the optical conductivity of the four mono- and few-layers TMD materials parametrized by the multi-Lorentzian dispersion relation defined by Eq. (1). The oscillator strength f_k, the spectral resonance energy E_k, and the spectral width γ_k of the *k*-th oscillator are given in eV^2, eV, and eV, respectively.

k	MoS_2			WS_2			$MoSe_2$			WSe_2		
	E_k (eV)	f_k (eV^2)	γ_k (eV)	E_k (eV)	f_k (eV^2)	γ_k (eV)	E_k (eV)	f_k (eV^2)	γ_k (eV)	E_k (eV)	f_k (eV^2)	γ_k (eV)
1	1.85	0.25	0.06	2.05	1.2	0.05	1.55	0.4	0.043	1.63	1.75	0.1
2	2.05	1.0	0.1	2.43	0.75	0.08	1.8	0.9	0.097	2.18	4.0	0.27
3	2.77	35	0.4	2.77	9	0.25	2.33	10	0.5	2.57	15.5	0.525
4	2.27	10	1.2	3.07	6	0.3	2.9	37.5	0.92	3.09	26.5	0.65
5	3.35	80	0.95	4.9	75	0.9	4.15	61	1.5	3.8	50	1.25
6	5.1	180	1.3	3.65	100	1.75				5.5	150	2.75

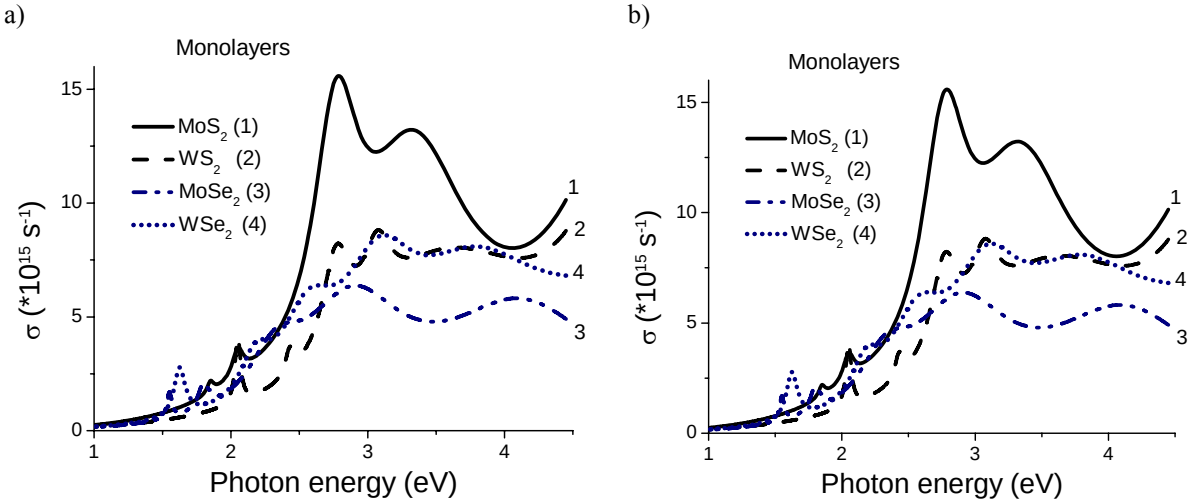

Fig. 5. (a) Modelling dispersion of the real part of optical conductivity for four low-dimensional TMD materials. (b) Emerging photoluminescence in mono- and few-layers at room temperature: MoS_2, WS_2, $MoSe_2$, and WSe_2.

Photoluminescence. Strong photoluminescence is observed in the chemically exfoliated mono- and few-layers, which indicates that they are close to direct gap semiconductors in agreement with the recent experimental findings [25] and calculations [34]. Photoluminescence (PL) emission of mono- and few-layers MoS_2, $MoSe_2$, WS_2, and WSe_2 is investigated and presented in Fig. 5b. The emission spectra for the MoS_2 sheets consist of one major peak and one minor peak around 1.84 and 1.97 eV, respectively. The observed emission lines for monolayer MoS_2 are in good agreement with the known direct A and B excitons (Fig. 1) in the corresponding monolayer, suggesting that they are from the direct band gap photoluminescence from K point. Fig. 5b shows prominent PL of monolayer WS_2 centered at 1.91 eV. The PL spectra for the $MoSe_2$ and WSe_2 (Fig. 5b) monolayers are dominated by exciton peaks at 1.57 and 1.65 eV, respectively. The emission from these monolayers exhibits broader maxima than that for the WS_2 (Fig. 5b). These observations corroborate recent photoluminescence data of monolayer MoS_2, $MoSe_2$, WS_2, and WSe_2 [25, 41, 42]. These four materials possess indirect bandgap in bulk and become the direct bandgap ones in the 2D limit. From our ellipsometric and PL measurements, we can conclude that monolayer WS_2 has the largest direct band gap of about ~2.2 eV. It decreases down to ~1.9, ~1.8, and ~1.6 eV for mono- and few-layers MoS_2, WSe_2, and $MoSe_2$, respectively. Our results are close to the values reported by PL experiments in mechanically exfoliated monolayer MoS_2, [25, 41, 43] $MoSe_2$, WS_2, and WSe_2 [25, 42].

4. Conclusion

The complex optical constants of chemically exfoliated mono- and few-layers of two-dimensional materials, namely: MoS_2, $MoSe_2$, and WS_2, WSe_2 transition metal dichalcogenides, have been measured using variable angle spectroscopic ellipsometry and transmission spectroscopy. We have confirmed the monolayer nanostructure of liquid exfoiliated TDMs materials by testing them by using high-resolution Raman spectroscopy and revealing strong photoluminescence emission at room temperature. Complex refractive indices as well as optical conductivity have been extracted from angle-variable ellipsometric dependences. Comparisons to associated bulk responses reveal differences caused by increased electron-hole interactions in mono- and few-layers of TMDs. Very clear excitonic absorption peaks A and B were found in the red region for all monolayer TMDs. They originate from the spin-split direct gap transitions at the K point of the Brillouin zone. In addition to the lower energy exciton peaks, a series of higher energy ($E >$ 2.5 eV) sharp peaks are observed in the optical spectra of confined TMDs nanostructures. We believe that the optical features reported here will stimulate further investigations of the electronic structure of transition metal dichalcogenides monolayers and provide better understanding the optical responses of TMDs to their optoelectronic device designs and applications as solar accumulating nanostructures.

References

1. Geim A.K. and Grigorieva I.V. Van der Waals heterostructures. *Nature*. 2013. **499**. P. 419–425.
2. Novoselov K.S., Mishchenko A., Carvalho A., Castro Neto A.H. 2D materials and van der Waals heterostructures. *Science*. 2016. **353**. P. 6298.
3. Mak K.F., Lee C., Hone J., Shan J., and Heinz T.F. Atomically thin MoS_2: A new direct-gap semiconductor. *Phys. Rev. Lett.* 2010. **105**. P. 136805.

4. Chernikov A., Berkelbach T.C., Hill H.M., Rigosi A., Li Y., Aslan O.B., Reichman D.R., Hybertsen M.S., and Heinz T.F. Exciton binding energy and nonhydrogenic Rydberg series in monolayer WS_2. *Phys. Rev. Lett*. 2014. **113**. P. 076802.
5. Cudazzo P., Sponza L., Giorgetti C., Reining L., Sottile F., and Gatti M. Exciton band structure in two-dimensional materials. *Phys. Rev. Lett.* 2016. **116**. P. 066803.
6. Trushin M., Goerbig M.O., and Belzig W. Optical absorption by Dirac excitons in single-layer transition-metal dichalcogenides. *Phys. Rev. B*. 2016. **94**. P. 041301.
7. Gourmelon E., Lignier O., Hadouda H., Couturier G., Bernède J.C., Tedd J., Pouzet J. and Salardenne J. MS_2 (M = W, Mo) photosensitive thin films for solar cells. *Sol. Energy Mater. Sol. Cells*. 1997. **46**. P. 115-121.
8. Lopez-Sanchez O., Llado E.A., Koman V., Fontcuberta A., Morral I., Radenovic A., and Kis A. Light generation and harvesting in a van der Waals heterostructure. *ACS Nano*. 2014. **8**. P. 3042–3048.
9. Beard M.C., Luther J.M., and Nozik A.J. The promise and challenge of nanostructured solar cells. *Nature Nanotechnol*. 2014. **9**. P. 951–954.
10. Kuryoz P.Yu., Poperenko L.V., and Kravets V.G. Correlation between dielectric constants and enhancement of surface plasmon resonances for thin gold films. *phys. status solidi* (a). 2013. **210**. P. 2445–2455.
11. Makinistian L., Albanesi E.A., Gonzalez Lemus N.V. et al. Ab initio calculations and ellipsometry measurements of the optical properties of the layered semiconductor In_4Se_3. *Phys. Rev. B*. 2010. **81**. P. 075217.
12. Kravets V.G., Grigorenko A.N., Nair R.R., Blake P., Anissimova S., Novoselov K.S., and Geim A.K. Spectroscopic ellipsometry of graphene and an exciton-shifted van Hove peak in absorption. *Phys. Rev. B*. 2010. **81**. P. 155413.
13. Rozouvan T., Poperenko L., Kravets V., Shaykevich I. Enhancement of absorption in vertically-oriented graphene sheets growing on a thin copper layer. *Appl. Surf. Sci*. 2017. **396**. P. 1–7.
14. Yim C., O'Brien M., McEvoy N., Winters S., Mirza I., Lunney J.G., and Duesberg G.S. Investigation of the optical properties of MoS_2 thin films using spectroscopic ellipsometry. *Appl. Phys. Lett*. 2014. **104**. P. 103114.
15. Li Y., Chernikov A., Zhang X., Rigosi A., Hill H.M., van der Zande A.M., Chenet D.A., Shih E.-M., Hone J., and Heinz T.F. Measurement of the optical dielectric function of monolayer transition-metal dichalcogenides: MoS_2, $MoSe_2$, WS_2, and WSe_2. *Phys. Rev. B*. 2014. **90**. P. 205422.
16. Morozov Yu.V. and Kuno M. Optical constants and dynamic conductivities of single layer MoS_2, $MoSe_2$, and WSe_2. *Appl. Phys. Lett*. 2015. **107**. P. 083103.
17. Chhowalla M., Shin H.S., Eda G., Li L.-J., Loh K.P. and Zhang H. The chemistry of two-dimensional layered transition metal dichalcogenide nanosheets. *Nat. Chem*. 2013. **5**. P. 263–275.
18. Halim U., Zheng C.R., Chen Y., Lin Z., Jiang S., Cheng R., Huang Y. and Duan X. A rational design of cosolvent exfoliation of layered materials by directly probing liquid–solid interaction. *Nat. Commun*. 2013. **4**. P. 2213.
19. Beattie J.R. Optical constants of metals. *J. Phil. Mag*. 1955. **46**. P. 235–245.
20. Azzam R.M.A. and Bashara N.M. *Ellipsometry and Polarized Light*. North-Holland, Amsterdam, 1977.
21. Kravets V.G., Petford-Long A.K., Kravets A.F. Optical and magneto-optical properties of $(CoFe)_x(HfO_2)_{1-x}$ magnetic granular films. *J. Appl. Phys*. 2000. **87**. P. 1762–1768.
22. Born M. and Wolf E. *Principles of Optics*. Cambridge University Press, Cambridge, England, 1999.
23. Wooten Frederick, *Optical Properties of Solids*. New York and London: Academic Press, 1972.
24. Mennicke R.T., Bozec D., Kravets V.G. *et al*. Modelling the magneto refractive effect in giant magnetoresistive granular and layered materials. *J. Magn. Mag. Mat.* 2006. **303**. P. 92–110.
25. Tonndorf P., Schmidt R., Bouttger P., Zhang X., Bourner J., Liebig A., Albrect M., Kloc Ch., Gordan O., Zahn D.R.T., de Vasconcellos S.M., Bratschitsch R. Photoluminescence emission and Raman response of monolayer MoS_2, $MoSe_2$, and WSe_2. *Opt. Exp.* 2013. **21**. P. 4908–4916.
26. Li H., Zhang Q., Yap C.C.R., Tay B.K., Edwin T.H.T., Olivier A., and Baillargeat D. From bulk to monolayer MoS_2: evolution of Raman scattering. *Adv. Funct. Mater*. 2012. **22**. P. 1385–1390.
27. Molina-Sánchez A. and Wirtz L. Phonons in single-layer and few-layer MoS_2 and WS_2. *Phys. Rev. B*. 2011. **84**. P. 155413.
28. Ramasubramaniam A. Large excitonic effects in monolayers of molybdenum and tungsten dichalcogenides. *Phys. Rev. B*. 2012. **86**. P. 115409.
29. Eichfeld S.M., Eichfeld C.M., Lin Yu-C., Hossain L. and Robinson J.A. Rapid, non-destructive evaluation of ultrathin WSe_2 using spectroscopic ellipsometry. *APL Materials*. 2014. **2**. P. 092508.
30. Ding Y., Wang Y., Ni J., Shi L., Shi S., and Tang W. First principles study of structural, vibrational and electronic properties of graphene-like MX2 (M = Mo, Nb, W, Ta; X = S, Se, Te) monolayers. *Physica B*. 2011. **406**. P. 2254–2260.
31. Sundaram R.S., Engel M., Lombardo A., Krupke R., Ferrari A.C., Avouris P., and Steiner M.

Electroluminescence in single layer MoS_2. *Nano Lett*. 2013. **13**. P. 1416–1421.
32. Bonaccorso F., Sun Z., Hasan T. & Ferrari A.C. Graphene photonics and optoelectronics. *Nature Photon*. 2010. **4**. P. 611–622.
33. Wilson J.A., Yoffe A.D. The transition metal dichalcogenides discussion and interpretation of the observed optical, electrical and structural properties. *Adv. Phys*. 1969. **18**. P. 193−335.
34. Kuc A., Zibouche N., Heine T. Influence of quantum confinement on the electronic structure of the transition metal sulfide TS_2. *Phys. Rev. B*. 2011. **83**. P. 245213.
35. Consadori F., Frindt R.F. Crystal size effects on the exciton absorption spectrum of WSe_2. *Phys. Rev. B*. 1970. **2**. P. 4893–4896.
36. Cao T., Wang G., Han W., Ye H., Zhu C., Shi J., Niu Q., Tan P., Wang E., Liu B., and Feng J. Valley-selective circular dichroism of monolayer molybdenum disulphide. *Nat. Commun*. 2012. **3**. P. 887.
37. Komsa H.P. and Krasheninnikov A.V. Effects of confinement and environment on the electronic structure and exciton binding energy of MoS_2 from first principles. *Phys. Rev. B*. 2012. **86**. P. 241201(R).
38. Molina-Sànchez A., Sangalli D., Hummer K., Marini A., and Wirtz L. Effect of spin-orbit interaction on the optical spectra of single-layer, double-layer, and bulk MoS_2. *Phys. Rev. B*. 2013. **88**. P. 045412.
39. Shen C.-C., Hsu Y.-T., Li L.-J., and Liu H.-L. Charge dynamics and electronic structures of monolayer MoS_2 films grown by chemical vapor deposition. *Appl. Phys. Exp*. 2013. **6**. P. 125801.
40. Yu P.Y. and Cardona M. *Fundamental of Semiconductors: Physics and Materials Properties*, 2nd ed. Berlin: Springer, 1999.
41. Splendiani A., Sun L., Zhang Y., Li T., Kim J., Chim C.-Y., Galli G., and Wang F. Emerging photoluminescence in monolayer MoS_2. *Nano Lett.* 2010. **10**. P. 1271–1275.
42. Huang Ch., Wu S., Sanchez A.M., Peters J.J.P., Beanland R., Ross J.S., Rivera P., Yao W., Cobden D.H., Xu X. Lateral heterojunctions within monolayer $MoSe_2$-WSe_2 semiconductors. *Nature Materials*. 2014. **13**. P. 1096–1101.
43. Eda G., Yamaguchi H., Voiry D., Fujita T., Chen M., and Chhowalla M. Photoluminescence from chemically exfoliated MoS_2. *Nano Lett*. 2011. **11**. P. 5111–5116.